Isospin-spin excitations in the $A = 58$ mass region: The ^{58}Ni(^{3}He,t)^{58}Cu reaction

D. R. Bes and O. Civitarese
Laboratorio Tandar, CAC, CNEA, Av. Gral. Paz 1499, 1650 Partido de Gral, San Martiín, Argentina and
Department of Physics, University of La Plata, c. c. 67 1900, La Plata, Argentina
(Received 24 July 2006; revised manuscript received 10 April 2008; published 24 July 2008)

The experimental information on isospin-spin excitations around ^{58}Ni is analyzed by using isoscalar and isovector pairing vibrations, Gamow-Teller (GT) modes, and their couplings. It is found that the proposed coupling scheme accounts for a sizable amount of the strength associated with isospin-spin excitations, which include transitions to both one- and two-phonon states. The calculations are performed within the framework of perturbation theory, accounting for the renormalization of the charge by the collective GT excitations.

DOI: 10.1103/PhysRevC.78.014317 PACS number(s): 21.60.Fw, 21.30.Fe, 24.30.Gd, 27.40.+z

I. INTRODUCTION

The experimental study of nuclear isospin-spin responses to charge-exchange reactions has received considerable attention during recent years [1]. These experiments are particularly relevant to studies of specific nuclear isospin-spin dependent processes, such as neutrino-induced reactions and exotic electroweak decays. The (^{3}He,t) and (p, n) reactions are the obvious choices for exploring isospin-spin dependent excitations, and they have been used as experimental tools for large-scale nuclear structure studies [1,2].

A typical energy spectrum of tritons from (^{3}He,t) reactions on medium-heavy nuclei displays the narrow peak corresponding to the isobaric analog state (IAS) and the broad strength distribution of the Gamow-Teller resonance (GTR). Studies on ^{58}Cu [3,4] show, in addition, the existence of four $T = 1, I = 1$ states and a high-energy spin-dipole resonance. In this paper, we take the results of Ref. [3] as our main motivation. In the case of (p, n) reactions, the energy spectrum also shows the presence of spin-dipole resonances. All these excitations participate in low-energy charge-exchange, β-decay, and electron-capture processes [1,5,6].

From the point of view of nuclear structure models, the collectivity of spin dependent modes was studied in the framework of nuclear vibrations [7]. This description is similar to the one applied to electric multipole excitations. In this context, isospin-spin dependent excitations are described as the linear superposition of particle-hole (two quasiparticles) proton-neutron configurations. Some features of the experimental spectra, such as energy centroids, are well reproduced by the vibrational model; but some others, such as the strength distributions, are predicted with less accuracy. Particularly, the strength of the Gamow-Teller (GT) transitions is not reproduced unless the operator responsible for the transitions is renormalized [8,9]. Moreover, the detailed identification of the excitations in terms of their spin-isospin structure turns out to be rather difficult. Similar problems are encountered in shell model calculations, which are unable to reach the high-energy region of the charge-exchange and (^{3}He,t) spectra [10], although recent improvements have extended the range of applicability of the shell model [11].

This paper analyzes the available experimental information for small spin S and isospin T states in nuclei near closed shells. A fairly successful analysis of the isovector pairing (IVP) degree of freedom has been made already for the region around ^{56}Ni [12]. In the present work, we review the evidence concerning this coupling scheme, including odd-A nuclei, and we extend this analysis to $I^\pi = 1^+$ states. Therefore, in Sec. II and in Appendix A, we study those states which may be interpreted either as members of isoscalar pairing (ISP) multiplets or as GT excitations of closed shells. This is in contrast to the usual treatments of isoscalar pairing as an extension of the BCS formalism, which are handicapped due to the vicinity of the phase transition.

The main part of the paper is focused on GT transitions in ^{58}Ni. Use is made of the rules of the nuclear field theory (NFT) of Refs. [13,14]. In this perturbation framework, diagrams are ordered according to the power of a parameter ξ^{-1} which measures the number of pairs of single-particle excitations contributing to the collective modes.[1] The calculation is carried out to the lowest order of the parameter yielding a nonvanishing contribution. Since ξ is rather small in the region around ^{56}Ni, we cannot expect a very good convergence of the perturbative calculation. Moreover, the accuracy of the expansion may also be marred by accidental degeneracies. Nevertheless, we consider it worthwhile to analyze the empirical evidence in terms of the present point of view, since this is a difficult region for the theoretical analysis, where every treatment presents its own shortcomings.

Renormalization diagrams are obtained by replacing the GT vertices by particle-phonon vertices, the GT phonon being created (destroyed) at an earlier (later) time. It turns out that they are essential in order to preserve the Ikeda sum rule, which is necessarily violated by using the same effective charge for all GT transitions within a given shell. In the present paper, we develop the necessary formalism in order to account for renormalization effects.

The microscopic formalism is presented in Sec. III and Appendix B, where we review the essentials of the IVP, ISP, and GT excitations and their couplings. In Sec. IV, we apply the formalism to GT transitions. The calculation of renormalization diagrams is treated in Appendix C, with

[1]The simultaneous treatment of pairing and particle-hole phonons has been performed in Ref. [14] for a schematic model.

special care for transitions to the giant GT resonance (Sec. V and Appendix D). In Sec. VI, we predict the population of final states in the reaction ^{58}Ni(^{3}He,t)^{58}Cu. Conclusions are drawn in Sec. VII.

II. MACROSCOPIC FRAMEWORK

We identify the vacuum state $|\,\rangle$ as the double-closed shell nucleus ^{56}Ni with spin $I = 0$ and isospin $T = 0$. Fermion excitations are created either by application of proton (neutron) annihilation operators $b_{hm}\,(c_{hm})$ or by creation operators $b^+_{km}(c^+_{km})$. The labels h, k denote the quantum numbers specifying the single-particle states, including the angular momentum but excluding the magnetic quantum number.

We also take into account three boson degrees of freedom, labeled by the angular momentum quantum numbers I, M, the isospin T, T_z, and the pair-transfer number $\alpha = 0, \pm 1$. The quantum number ν orders the states with the previous labels in common. Thus, phonon creation operators are denoted by $\Gamma^+_{IM,TT_z,\alpha,\nu}$ and the corresponding energies by $\omega_\nu^{IT\alpha}$.

As in Ref. [12], we have collected the empirical evidence concerning the energies for the IVP coupling scheme. Figure 1 displays the values of the energies

$$K(i, A, T) = E(i, A, T) + B_e(56, 0) - B_w(56, 0) - B_e(A, T) + B_w(A, T). \quad (1)$$

The quantity $E(i, A, T)$ is the "true" excitation energy relative to the ground state (g.s.) of the nucleus with isospin quantum numbers T, $T_z = -T$, while $K(i, A, T)$ is the "model" energy representing excitation energies relative to the ground state of ^{56}Ni that are deprived from alien contributions to the model. In Eq. (1), $B_e(A, T)$ is the experimental binding energy of the g.s. of the nucleus with A, T. The quantity $B_w(A, T)$ is defined through the Weizsäcker mass formula

$$B_w(A, T) = b_v A - 17A^{2/3} - 2b_s T(T + 1)/A - 0.7\, Z(Z - 1)(1 - 0.76/Z^{2/3})/A^{1/3}, \quad (2)$$

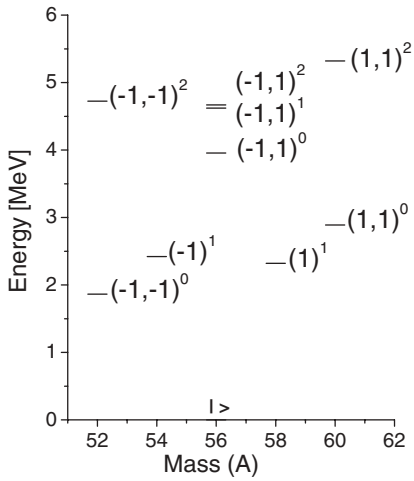

FIG. 1. Even-mass states around $A = 56$. The transfer quantum number of the phonons is indicated in parenthesis. The total isospin of the states is given in the upper right-hand corner of the parenthesis of each configuration.

where $Z = \frac{1}{2}A - T$. All terms are given in units of MeV. The parameter b_v is chosen to be 15.5 MeV, thus ensuring that the energies of the first excited isovector pairing modes $\Gamma^+_{00,1(-1)\pm1,1}$ satisfy $\omega_1^{01(-1)} \approx \omega_1^{011}$. It constitutes a small departure from the traditional value $b_v = 16$ MeV. This difference has no physical consequences.

The symmetry term contains a potential and a kinetic contribution. Of the two, only the potential term should be subtracted from the experimental energy, since it is associated with features of the nuclear interaction not connected with the present model space. Since both potential and kinetic terms are of similar size, we use $b_s \approx 25$ MeV, as in Ref. [12].

It turns out that the most abundant information concerns IVP phonons ($I = 0$, $T = 1$, $\alpha = \pm 1$). The previous evidence on the vibrational character of this collective motion is further confirmed through its application to odd-mass nuclei (see Appendix A). On top of this basic structure we locate the $I = 1$ phonons, either ISP ($T = 0, \alpha = \pm 1$) or GT ($T = 1, \alpha = 0$). The available evidence on two-phonon states also supports the vibrational interpretation for the ISP modes (Appendix A).

III. MICROSCOPIC PHONON STRUCTURE

We define the following pairs of single-particle operators coupled to good angular momentum I and isospin T

$$[a^+_{j_1}a^+_{j_2}]^{I=0\,T=1}_{0T_z}; \quad [a^+_{j_1}a^+_{j_2}]^{10}_{M0}; \quad [a^+_{j_1}a_{j_2}]^{11}_{MT_z}. \quad (3)$$

Here a^+_j is either $= b^+_j$ or c^+_j and $j = k, h$. We construct the operators $P^+_{IM,TT_z,\alpha}$

$$\begin{aligned} P^+_{IM,TT_z,1} &= f^{IT1}_{j_1j_2}\left[a^+_{j_1}a^+_{j_2}\right]^{IT}_{MT_z}, \\ P^+_{1M,1T_z,0} &= f^{110}_{j_1j_2}\left[a^+_{j_1}a_{j_2}\right]^{11}_{MT_z}, \\ P^+_{IM,TT_z,-1} &= (-1)^{I+T+M+T_z} P_{I(-M),T(-T_z),1}, \end{aligned} \quad (4)$$

where

$$f^{01(\pm1)}_{j_1j_2} = \delta_{j_1j_2}\,\hat{j}_1; \quad f^{10(\pm1)}_{j_1j_2} = f^{110}_{j_1j_2} = \frac{\langle j_1||\sigma||j_2\rangle}{\sqrt{3}}. \quad (5)$$

We assume separable residual interactions of the form

$$H^{IT\alpha} = -\frac{g^{IT\alpha}}{1 + \delta_{\alpha0}}\, P^+_{IM,TT_z,\alpha}\, P_{IM,TT_z,\alpha}. \quad (6)$$

A subset of the paired operators in Eq. (3) have a boson-like behavior, giving rise to the (normalized) coupled boson creation operators $\gamma^+_{IM,TT_z,\alpha;j_1j_2}$ (see Table I). We transform as usual to uncoupled bosons

$$\Gamma^+_{IM,TT_z,\alpha;\nu} = \lambda^{IT\alpha}_{\nu;j_1j_2}\,\gamma^+_{IM,TT_z,\alpha;j_1j_2} - (-1)^{I+M+T+T_z}\,\mu^{IT\alpha}_{\nu;j_1j_2}\,\gamma_{I(-M),T(-T_z);-\alpha;j_1j_2}. \quad (7)$$

The $P^+_{IM,TT_z,\alpha}$ operators in Eq. (4) have a collective version, which is obtained through the inversion of Eq. (7) and its

TABLE I. Coupled phonons used in the present work.

$\gamma^+_{00,11,1;kk} = [b^+_k b^+_k]^0$	$\gamma^+_{00,11,-1;hh} = -[c_h c_h]^0$
$\gamma^+_{00,10,1;kk} = [b^+_k c^+_k]^0$	$\gamma^+_{00,10;-1;hh} = [b_h c_h]^0$
$\gamma^+_{00;1(-1),1;kk} = [c^+_k c^+_k]^0$	$\gamma^+_{00,1(-1),-1;hh} = -[b_h b_h]^0$
$\gamma^+_{1M,00,1;k_1k_2} = [b^+_{k_1} c^+_{k_2}]^1_M$	$\gamma^+_{1M,00,-1;h_1h_2} = -[b_{h_1} c_{h_2}]^1_M$
$\gamma^+_{1M,11,0;kh} = -[b^+_k c_h]^1_M$	$\gamma^+_{1M,10,0;kh} = \frac{1}{\sqrt{2}}([b^+_k b_h]^1_M - [c^+_k c_h]^1_M)$
$\gamma^+_{1M,1(-1),0;kh} = [c^+_k b_h]^1_M$	

insertion into Eq. (4),

$$(P^+_{IM,TT_z,\alpha})_{\rm coll} = \frac{\Xi^{IT\alpha}_\nu}{g^{IT\alpha}} \Gamma^+_{IM,TT_z,\alpha;\nu} + \frac{\Xi^{IT(-\alpha)}_\nu}{g^{IT(-\alpha)}} (-1)^{I+M+T+T_z} \Gamma_{I(-M),T(-T_z),-\alpha;\nu}. \quad (8)$$

The pairing strengths $g^{IT(\pm1)}$ are determined from the lowest state of the systems with $A = 54$ and 58, and with $I = 0$ and 1. Using these strengths, we obtain the parameters corresponding to the different roots of the random-phase approximation (RPA) equations (B1). They are listed in Table II. We fix $\omega^{110}_1 = 7.00$ MeV, a value that is about 20% higher than the lowest $[c^+_{5/2} c_{7/2}]^1_M$ particle-hole state and consistent with the systematics of GT resonances. See also Appendix A. The corresponding collective parameter Ξ^{110}_1 is also given in Table II.

As a consequence of the simultaneous existence of particle and phonon subspaces, there appear particle-vibration coupling terms

$$H_{\rm pv} = -\frac{g^{IT\alpha}}{1+\delta_{\alpha0}} ((P^+_{IM,TT_z,\alpha})_{\rm coll} P_{IM,TT_z,\alpha} + P^+_{IM,TT_z,\alpha} (P_{IM,TT_z,\alpha})_{\rm coll}). \quad (9)$$

TABLE II. Parameters of the phonons entering in the calculation. Energies $\omega^{IT\alpha}_\nu$, coupling strengths $g^{IT\alpha}_\nu$, and vertex factors $\Xi^{IT\alpha}_\nu$ are in MeV.

I	T	α	ν	$g^{IT\alpha}$	$\omega^{IT\alpha}_\nu$	$\Xi^{IT\alpha}_\nu$
0	1	1	1	0.387	2.34	1.42
			2		5.61	0.38
			3		6.83	0.077
0	1	−1	1	0.402	2.42	1.52
			2		15.38	0.69
			3		18.55	0.33
			4		23.32	0.55
1	0	1	1	0.171	3.84	.50
			2		5.32	0.21
			3		6.38	0.092
			4		6.89	0.036
1	0	−1	1	0.212	4.17	0.58
			2		16.02	0.39
			3		17.94	0.52
			4		19.51	0.26
			5		23.92	0.24
1	1	0	1	−0.272	7.00	0.53

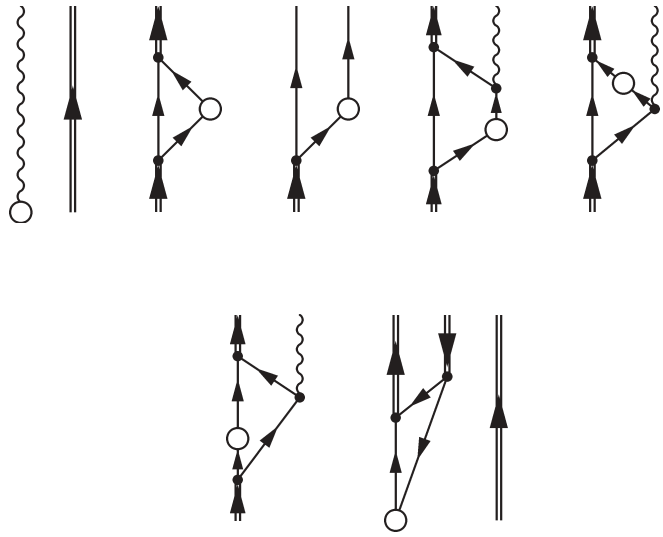

FIG. 2. Elementary processes accounted for in the perturbative treatment of GT transitions. From left to right, upper row: diagrams 0, A, B, C and F, D and G; lower row: E and H, I and J. Lines represent particles or holes (single lines), particle-hole phonons (arrowed wavy lines), and two-particle phonons (arrowed double lines). Open circles represent the action of the transition operator Q; solid dots represent the interactions between particles and phonons.

They give rise to the particle-vibration vertices appearing in the diagrammatic treatment [13].

Within the NFT [13], the magnitude of the diagrams is fixed by the fact that each particle-vibration factor $\Xi^{IT\alpha}_\nu$ is of order $\mathcal{O}(\xi^{-1/2})$; each strength parameter $g^{IT\alpha}$, of $\mathcal{O}(\xi^{-1})$; and a factor $\mathcal{O}(\xi)$ is present for each fermion loop. For diagrams yielding transition amplitudes, an insertion of the GT operator of Eq. (10) is of $\mathcal{O}(\xi^0)$, while the creation or annihilation of the collective phonon in Eq. (8) introduces a factor $\mathcal{O}(\xi^{1/2})$.

IV. GAMOW-TELLER TRANSITIONS

In the following we describe the matrix elements of the GT operator in the presence of pairing and GT vibrations. We consider the operator

$$Q_{1M} \equiv P^+_{1M,11,0} = -\frac{\langle j'||\sigma||j\rangle}{\sqrt{3}} [b^+_{j'} c_j]^1_M . \quad (10)$$

The simpler diagrammatic contributions to GT transitions are represented in Fig. 2. All final states have $T_z = 0$. The matrix elements of the GT operator to final states with good isospin are

$$\kappa^{T=0}_{A\nu} = \langle \Gamma^+_{1M,00,1;\nu} | Q_{1M} | 0\rangle, \quad (11)$$

$$\kappa^{T=1}_B = \frac{1}{\sqrt{2}} \langle [b^+_{\frac{3}{2}-} c^+_{\frac{1}{2}-}]^1_M - [b^+_{\frac{1}{2}-} c^+_{\frac{3}{2}-}]^1_M | Q_{1M} | 0\rangle, \quad (12)$$

$$\kappa^{T=1}_{C\nu}, \kappa^{T=1}_{D\nu}, \kappa^{T=1}_{E\nu} = \langle [\Gamma^+_{1,00,1;\nu} \Gamma^+_{1,10,0;1}]^1_M | Q_{1M} | 0\rangle_{C,D,E}. \quad (13)$$

TABLE III. Expressions for the numerators of the graphs represented in Fig. 2.

Graph	Final state	Value of numerator
A	$\Gamma_{1M,00,1;\nu}\|\rangle$	$(f^{101}_{j_1j_2})^2\,\Xi^{101}_{\nu}\;\Xi^{011}_{1}$
B	$\frac{1}{\sqrt{2}}\left([b^+_k c^+_{k_2}]^1_M - [b^+_{k_2} c^+_k]^1_M\right)\|\rangle$	$\frac{1}{2} f^{101}_{j_1j_2}\;\Xi^{011}_{1}$
C,D,E	$[\Gamma^+_{1,10,0;1}\Gamma^+_{1,00,1;\nu}]^1_M\|\rangle$	$\rho = \frac{3}{\sqrt{2}} f^{101}_{j_1j_3} f^{101}_{j_3j_2} f^{101}_{j_2j_1} \begin{Bmatrix} 1 & j_3 & j_2 \\ j_1 & 1 & 1 \end{Bmatrix} \Xi^{011}_{1}\,\Xi^{110}_{1}\,\Xi^{101}_{\nu}$
F,G,H	$\Gamma^+_{1M,11,0;1}\,\Gamma^+_{00,1(-1),1;\nu}\|\rangle$	$\eta = (f^{101}_{j_1j_2})^2\,\Xi^{110}_{1}\;\Xi^{011}_{\nu}\,\Xi^{011}_{1}$
I	$\Gamma^+_{00,11,-1;\nu}\Gamma^+_{1M,00,1;\nu'}\|0\rangle$	$(f^{101}_{j_1j_2})^2\;\Xi^{01(-1)}_{\nu}\;\Xi^{101}_{\nu'}$
J	$\Gamma^+_{00,11,1;\nu}\Gamma^+_{1M,00,-1;\nu'}\|0\rangle$	$(f^{101}_{j_1j_2})^2\;\Xi^{011}_{\nu}\;\Xi^{10(-1)}_{\nu'}$

If, in addition to the GT phonon, the final pairing phonon is isovector instead of isoscalar, diagrams F, G, H allow us to calculate the following amplitudes:

$$\begin{aligned}
\kappa_{F\nu} &= \langle\Gamma^+_{1M,11,0;1}\Gamma^+_{00,1(-1),1;\nu}|Q_{1M}|0\rangle_F \\
&= -2\,\langle\Gamma^+_{1M,10,0;1}\Gamma^+_{00,10,1;\nu}|Q_{1M}|0\rangle_F, \\
\kappa_{G\nu} &= 2\,\langle\Gamma^+_{1M,10,0;1}\Gamma^+_{00,10,1;\nu}|Q_{1M}|0\rangle_G, \\
\kappa_{H\nu} &= \langle\Gamma^+_{1M,1(-1),0;1}\Gamma^+_{00,11,1;\nu}|Q_{1M}|0\rangle_H \\
&= -2\langle\Gamma^+_{1M,10,0;1}\Gamma^+_{00,10,1;\nu}|Q_{1M}|0\rangle_H.
\end{aligned} \tag{14}$$

Thus, the amplitudes for populating states with good isospin may be expressed as

$$\begin{aligned}
\kappa^T_{\nu} &= \langle[\Gamma^+_{1M,1,0;1}\Gamma^+_{00,1,1;\nu}]^T|Q_{1M}|0\rangle \\
&= \langle 11;1(-1);T0\rangle[(1-r_T)\,(\kappa_{F\nu}+(-1)^T\kappa_{H\nu})+r_T\,\kappa_{G\nu}],
\end{aligned} \tag{15}$$

where

$$r_T \equiv \frac{\langle 10;10;T0\rangle}{2\langle 11;1(-1);T0\rangle}. \tag{16}$$

However, if the final IVP state is the same as the initial one ($\nu = 1$), we must include also the amplitude due to the collective excitation of the GTR through Eq. (8) (diagram 0 in Fig. 2)

$$\begin{aligned}
&\langle[\Gamma^+_{1M,1,0;1}\Gamma^+_{00,1,1;1}]^T|Q_{1M}|0\rangle \\
&\quad= \langle 11;1(-1);T0\rangle\frac{\Xi^{110}_1}{g^{110}} + \kappa^T_1 \\
&\quad= \langle 11;1(-1);T0\rangle \\
&\qquad\times\left(\frac{\Xi^{110}_1}{g^{110}} + (1-r_T)\,(\kappa_{F1}+(-1)^T\kappa_{H1})+r_T\,\kappa_{G1}\right).
\end{aligned} \tag{17}$$

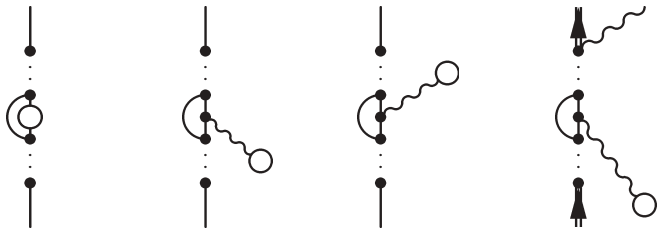

FIG. 3. Renormalization diagrams, numbered 1, 2, 3, and 4 from left to right.

Transitions to a final state composed of two addition and one removal pairing phonon (Fig. 2, diagrams I, J) are given by the matrix elements

$$\begin{aligned}
\kappa_I &= \langle(\Gamma^+_{1M,00,1;\nu}\Gamma^+_{00,11,-1;1})|Q_{1M}|0\rangle \\
\kappa_J &= \langle(\Gamma^+_{1M,00,-1;1}\Gamma^+_{00,11,1;\nu})|Q_{1M}|0\rangle.
\end{aligned} \tag{18}$$

In both cases, the matrix elements to states with good isospin are obtained by multiplying them by the proper Clebsch-Gordan coefficient

$$\kappa^T_{I,J} = \langle 11;1(-1);T0\rangle\,\kappa_{I,J}. \tag{19}$$

According to the NFT ordering of the diagrams, the amplitudes $\kappa_A, \kappa_B, \kappa_I, \kappa_J$ are of $\mathcal{O}(\xi^0)$, while $\kappa_C, \kappa_D, \kappa_E, \kappa_F, \kappa_G, \kappa_H$ are smaller, of $\mathcal{O}(\xi^{-1/2})$. However, for transitions to the GTR, the interference between the collective amplitude $\mathcal{O}(\xi^{1/2})$ and the second term $\mathcal{O}(\xi^{-1/2})$ in Eq. (17) acts as an amplifier. Therefore, the intensity due to the diagrammatic contributions of Eq. (14) to the excitation of the resonance becomes of $\mathcal{O}(\xi^0)$

$$\begin{aligned}
&|\langle[\Gamma^+_{1M,1,0;1}\Gamma^+_{00,1,1;1}]^T|Q_{1M}|0\rangle|^2 \\
&\quad= \langle 11;1(-1);T0\rangle^2\left(\left(\frac{\Xi^{110}_1}{g^{110}}\right)^2 + \frac{2\Xi^{110}_1}{g^{110}}\right. \\
&\qquad\left.\times[(1-r_T)(\kappa_{F1}+(-1)^T\kappa_{H1})+r_T\kappa_{G1}]\right),
\end{aligned} \tag{20}$$

where we neglect terms of $\mathcal{O}(\xi^{-1})$. Moreover, because of the orthogonality between Clebsch-Gordan coefficients, the total

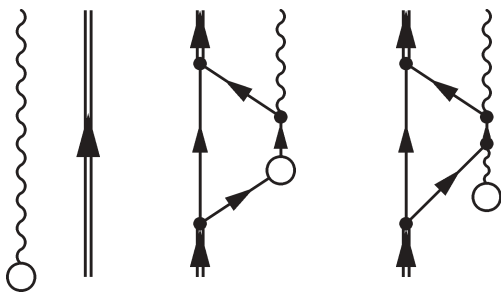

FIG. 4. Diagrams illustrating the action of the collective operator (open circles).

TABLE IV. Model energies and GT matrix elements to excited states with good isospin projection T_z, for the diagrams represented in Fig. 2. Only amplitudes yielding intensities larger than 0.01 are included.

Graph	ν	$K(i, A, T)$	$(\kappa_i)_{\text{bare}}$	$(\kappa_i)_{\text{ren}}$
A	1	3.84	1.21	0.83
	2	5.32	0.35	0.22
B		5.81	0.27	0.16
C	1	10.84	0.016	0.026
D	1	10.84	0.172	0.280
E	1	10.84	0.158	0.257
F	1	9.34	−0.281	−0.204
G	1	9.34	−0.725	0.020
H	1	9.34	0.021	−0.105

intensity of transitions (20) become

$$\sum_T |\langle [\Gamma^+_{1M,1,0;1}\Gamma^+_{00,1,1;1}]^T |Q_{1M}|0\rangle|^2 = \left(\frac{\Xi_1^{110}}{g^{110}}\right)^2 + \frac{2\Xi_1^{110}}{g^{110}}\kappa_{F1}. \tag{21}$$

The previous expressions are insufficient to account for the intensities to a given order. This is because we must also include renormalization diagrams. They are obtained from an original diagram, of Fig. 3, by replacing a GT vertex [Eq. (10)] with the insertion of a GT phonon created or destroyed at other times through the collective operator of Eq. (8) (Fig. 4). Thus, renormalization diagrams are of the same order as the original one. They are discussed with detail in Appendix C. The final result is that expressions (20) and (21) are still valid, provided we replace the bare amplitudes κ_{i1} obtained from Eq. (14) by their renormalized values in Eq. (C20).

The effect of renormalization diagrams is usually taken into account by using an effective charge, but this is justified only for low-lying states. In particular, this replacement is completely unjustified for transitions to states close to and above the GTR (see Appendix C).

V. IKEDA SUM RULE

As mentioned in the Introduction, one main difficulty with the use of a renormalized Gamow-Teller charge is the missing of a sizable fraction of the Ikeda sum rule[2]

$$\sum_i |\langle i, M|Q_{1M}|0\rangle|^2 - \sum_i |\langle i, M|\bar{Q}_{1M}|0\rangle|^2 = N - Z, \tag{22}$$

where Q_{1M} is given in Eq. (10) and

$$\bar{Q}_{1M} \equiv P^+_{1M,1(-1),0} = \frac{\langle j'||\sigma||j\rangle}{\sqrt{3}}[c^+_{j'}b_j]^1_M. \tag{23}$$

A collective phonon of Eq. (8) is also associated with the operator $\bar{Q}_{1M}$. The treatment of transitions from the initial state $|0\rangle$ is simpler than those due to Eq. (10), since Eq. (23) carries $T_z = -1$ and thus all states $\bar{Q}_{1M}|0\rangle$ carry $T = 2$. In fact, the only contribution is obtained from diagram G in Fig. 2 and its renormalizations.

Using Eq. (21), and its analog for $\bar{Q}_{1M}$, we note that the (large) term $(\Xi_1^{110}/g^{110})^2$ cancels in Eq. (22), and one is left with the contribution $[\mathcal{O}(\xi^0)]$

$$\frac{2\Xi_1^{110}}{g_1^{110}}(\kappa_{F1} - \kappa_{G1}), \tag{24}$$

where the renormalized values of κ_{F1}, κ_{G1} are given in Eq. (C20). The calculation of the sum rule requires the addition to Eq. (24) of intensities recorded in Table V populating states other than the GTR.

Applications to relevant schematic models are made in Appendix D. They verify the conservation of the Ikeda sum rule by the NFT treatment.

VI. RESULTS AND DISCUSSIONS

We apply the present treatment to the reaction ^{58}Ni(^{3}He,t)^{58}Cu. States populated through the GT operator of Eq. (10) may be described as single ISP states, a two-particle state with $I = 1$, $T = 0$, one ISP and one GT phonon, one IVP

[2]We appreciate the comments of one of the referees on this subject, which motivated the addition of the herein considerations and of Appendix D.

TABLE V. Predicted population of final states in ^{58}Cu through the reaction (^{3}He, t) on ^{58}Ni. The predicted "true" excitation energies $E(i, A, T)$ [see Eq. (1)] are in MeV. Only contributions larger than 0.01 are considered.

Final state $\|u\rangle$	ν	T	$E(i, A, T)$	$\|\langle u\|Q_{1M}\|0\rangle_{\text{bare}}\|^2$	$\|\langle u\|Q_{1M}\|0\rangle_{\text{ren}}\|^2$
$\Gamma^+_{1M,00,1;\nu}\|\,\rangle$	1	0	0.0	1.47	0.69
	2	0	1.48	0.12	0.05
$\frac{1}{\sqrt{2}}([b^+_{\frac{3}{2}-}c^+_{\frac{1}{2}-}]^1_M - [b^+_{\frac{1}{2}-}c^+_{\frac{3}{2}-}]^1_M)\|\rangle$		1	3.69	0.07	0.03
$[\Gamma^+_{1,1,0;1}\,\Gamma^+_{1,0,1;\nu}]^1_M\,\|\,\rangle$	1	1	8.72	0.12	0.32
$[\Gamma^+_{1M,1,0;1}\,\Gamma^+_{00,1,1;\nu}]^T\,\|\,\rangle$	1	0	7.20	1.30	1.88
	1	1	8.92	2.49	2.09
	1	2	12.36	1.10	0.42

TABLE VI. Single-particle model energies $K(i, A, T)$ [Eq. (1)] used in the calculation. The energies (in MeV) are average values resulting from the analysis of different isotopes.

Hole $(j\pi)$	$K(i, 55, \frac{1}{2})$	Particle$(j\pi)$	$K(i, 57, \frac{1}{2})$
$\frac{7}{2}^-$	2.62	$\frac{3}{2}^-$	2.35
$\frac{3}{2}^+$	8.19	$\frac{5}{2}^-$	3.24
$\frac{1}{2}^+$	9.45	$\frac{1}{2}^-$	3.46
$\frac{5}{2}^+$	12.16		

and one GT phonon, and two-addition–one-removal phonons. The calculated values of the matrix elements connecting the ground state $|0\rangle$ with these states are given in Table IV. The definitions of the matrix elements κ_i are given in Eqs. (13)–(16) and (18) for unrenormalized estimations and in Eqs. (C6) and (C20) for the estimations including renormalizations.

The intensities of transitions populating states of ^{58}Ni are calculated using the matrix elements listed in Table IV. The results are shown in Table V. To facilitate the comparison with experiments, true excitation energies $E(i, A, T)$ are used in this table. The last two columns in Table V are obtained by squaring the corresponding matrix elements of Table IV for transitions to a single ISP phonon or to the two-particle state with $I = 1, T = 0$. The square of the sum $\kappa_C + \kappa_D + \kappa_E$ is used for the population of a state composed of the ISP and the GTR. For the population of the IVP plus GTR states, we use expressions (20).

The renormalization yields sizable reductions to predictions for populating states lying below the GTR and corresponding increases in the predictions for states lying above the resonance. The amount of reduction for low-lying states is consistent with the empirical value $e_{\rm eff} \approx 0.8$ used in the literature. However, no single effective charge could have been used for the comparison between transitions populating states within a broader range of energies.

The predicted values corresponding to Eq. (24) are -1.73 and 0.87 for the bare and renormalized calculations, respectively. By adding these contributions to the first four lines of Table V, one obtains the values of the Ikeda sum rule 0.05 (unrenormalized) and 1.96 (renormalized).

In addition to the population of states listed in Tables VI and VII, the model predicts strong excitations of the three-phonon states

$$\Gamma^+_{1M,00,1;\nu}\,[\Gamma^+_{00,1,-1;1}\,\Gamma^+_{00,1,1;1}]^T\,|\rangle$$

TABLE VII. Predicted and experimental model energies of one-particle (hole)–one-phonon states.

A	Configuration	$K(i, A, T)^{\rm pred}$	$K^{\rm exp}_{T=\frac{1}{2}}$	$K^{\rm exp}_{T=\frac{3}{2}}$
53	$[a_{\frac{7}{2}^-}\,\Gamma^+_{0,1,-1;1}]^T$	5.03	4.00	5.36
55	$[a^+_{\frac{3}{2}^-}\,\Gamma^+_{0,1,-1;1}]^T$	4.78	5.23	4.73
57	$[a_{\frac{7}{2}^-}\,\Gamma^+_{0,1,1;1}]^T$	4.99	4.86	4.88
59	$[a^+_{\frac{3}{2}^-}\,\Gamma^+_{0,1,1;1}]^T$	4.74	3.74	4.94

and

$$\Gamma^+_{1M,00,-1;1}\,[\Gamma^+_{00,1,1;\nu}\,\Gamma^+_{00,1,1;1}]^T\,|\rangle \tag{25}$$

at 6.46 and 6.71 MeV, respectively. Unfortunately, it is not possible to calculate the magnitude of the relative intensities because of accidental degeneracies in the denominators, a fatal flaw of perturbation theory.

From the results in Table V, the calculated distribution of intensities shows isolated states below 5 MeV and a broad distribution from 7 to 12 MeV. The appearance of the broad distribution can therefore be explained as the result of the excitation of two-phonon states. The relative intensities of transitions to states belonging to these two energy regions are, roughly, in a ratio of 1:3 (unrenormalized matrix elements) or 1:6 (renormalized matrix elements). These features are consistent with the available data below 12 MeV. Above this energy, there are spin-dipole, negative parity excitations, which are not considered in the present calculation.

Since ours is a first nonvanishing order calculation we do not attempt to obtain the spreading width of each peak, which may be accounted for by four-particle two-hole admixtures to the GTR. We thus ensure that the first momentum of the strength distribution is accurately predicted (within the model). This is not the case of the spreading width, which is related to the second moment [15]. These effects could account for the population of the higher energy states experimentally observed.

Concerning the comparison between present and shell model calculations, it is worth mentioning that the two peaks found in the experiments, at 3.5 and 5.0 MeV, could correspond to the two predicted states in Eq. (25). These peaks were absent from shell model results [10]; however, the intensity around 6–7 MeV is predicted by the new shell model results [11].

VII. CONCLUSIONS

In this paper we have studied the response of ^{58}Cu to spin-isospin probes. The validity of the ISP and IVP vibrational model was tested against the low-lying spectrum of even and odd-mass nuclei around the double-closed shell, for one- and two-phonon states (even-mass nuclei) and one and two phonons coupled to active single-particle states. To this picture we added GT excitations.

The ground state of ^{58}Ni was interpreted as the low-lying one-phonon IVP excitation of the double-closed shell nucleus ^{56}Ni. Final 1^+ states in ^{58}Cu included both one ISP phonon and a superposition of GTR and pairing phonons. The calculation of transitions induced by the action of the isospin-spin probe was performed perturbatively within the framework of the RPA + NFT. Since vertices were extracted from the phenomenological analysis, the calculation was essentially parameter free.

We have developed the procedure to calculate renormalization diagrams, including those cases in which the GTR was populated. As a consequence of these diagrams, an effective charge was obtained for each transition. The departure from a single effective charge for all the shell is essential to preserve

the Ikeda sum rule, as was shown exactly for schematic models. It also was a satisfactory outcome of the realistic calculation.

Although the detailed comparison with data may be hampered by accidental numerical instabilities in the perturbative calculation of some of the states belonging to the high-energy portion of the spectrum, we are confident about the importance of the inclusion of pairing degrees of freedom in conjunction with GT excitations.

ACKNOWLEDGMENTS

This work has been partially supported by the National Research Council (CONICET) of Argentina.

APPENDIX A: EMPIRICAL EVIDENCE FOR PAIRING COUPLING SCHEMES

1. Elementary excitations

The "model" energies of the single-hole $a_{\frac{7}{2}}|\rangle$ and single-particle $a^+_{\frac{3}{2}}|\rangle$ states have been calculated using Eq. (1) and averaging over different isotopes (Table VI). The distances $e_{\frac{5}{2}^-} - e_{\frac{3}{2}^-} = 0.88$ and $e_{\frac{1}{2}^-} - e_{\frac{3}{2}^-} = 1.11$ MeV are obtained as an average of the excitation spectra in ^{57}Ni and ^{57}Cu. The distance between negative and positive parity, single-hole states is an educated guess, with very little physical consequences within the present calculation.

The one-phonon states $\Gamma^+_{00,1(-1),-1;1}$ and $\Gamma^+_{00,1(-1),1;1}$ have similar energies, 2.34 and 2.42 MeV, respectively, by construction. The adopted values quoted in Table II represent an average over the values corresponding to different isotopes. Since the GT interaction is repulsive, the energy $\omega_1^{110} \geq e_{\frac{5}{2}^-} + e_{\frac{7}{2}^-} = 5.86$ MeV. The closest empirical candidate is the 1^+ state in ^{56}Co, at an energy of 6.34 MeV. However, the model predicts two additional $I = 1, T = 1$ states at similar energies: the two-phonon states $\Gamma^+_{1M,00,-1;1}\,\Gamma^+_{00,1(-1),1;1}|\rangle$ and $\Gamma^+_{00,1(-1),-1;1}\,\Gamma^+_{1M,00,1;1}|\rangle$, at energies 6.50 and 6.25 MeV, respectively. It is difficult to distinguish between these possible interpretations through the population of the states, since the 1^+ state in ^{56}Co is populated by electron capture from ^{56}Ni or by charge-exchange reactions from ^{56}Fe (thus favoring the GTR assignment), but also by means of (^{3}He, p) and (α, d) transfer reactions on ^{54}Fe and (d, α) reactions on ^{58}Ni (favoring the two-pairing phonon interpretation). In view of these ambiguities, we have assigned the value $\omega_1^{110} = 7.00$ MeV, which is consistent with GTR systematics.

2. Energies of two-phonon and particle-phonon states

The positions of two-phonon and particle-phonon states test the vibrational description. The former lower states have the structure

$$\begin{aligned}
&[\Gamma^+_{00,1,-1;1}\,\Gamma^+_{00,1,-1;1}]^{T=0,2}|\rangle \quad (A = 52),\\
&[\Gamma^+_{00,1,-1;1}\,\Gamma^+_{00,1,1;1}]^{T=0,1,2}|\rangle \quad (A = 56),\\
&[\Gamma^+_{00,1,1;1}\,\Gamma^+_{00,1,1;1}]^{T=0,2}|\rangle \quad (A = 60).
\end{aligned} \tag{A1}$$

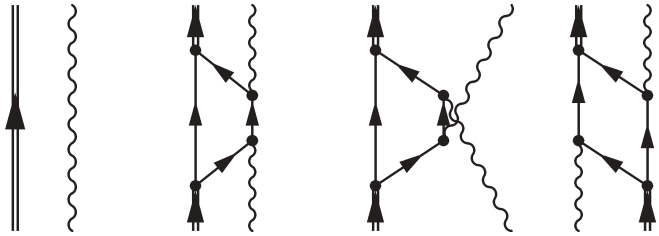

FIG. 5. Diagrammatic corrections to the energy of the two-phonon state. From left to right: unperturbed energy and diagrams F, G, and H.

The evidence supports the vibrational description for the three isospin states constructed with nonidentical phonons in the $A = 56$ system and for the states $T = 2$ built up with two identical phonons, in $A = 52$ and $A = 60$. However, the attractive interaction between proton and neutron particles (holes) lowers the energy for $T = 0$ states in the $A = 52$, 60 systems. The picture is quite symmetrical around $A = 56$.

The coupling scheme may be further tested through the inclusion of odd-mass nuclei.

Only states constructed with one particle (hole) and one phonon appear in Table VII. The model reproduces, within expectations, the experimental values of the energies, their smooth mass dependence, the alternate sequence of the angular momenta $I = \frac{7}{2}, \frac{3}{2}$, and the symmetry relative to $A = 56$. As for the case of $T = 0$, two-phonon states, there is a decrease in energy for the lowest value of T ($T = \frac{1}{2}$) if the odd hole is coupled to the removal phonon ($A = 53$) or if the odd particle is coupled to the addition phonon ($A = 59$).

Figure 6 displays the states obtained by coupling either a hole or a particle to the two-phonon states that were discussed

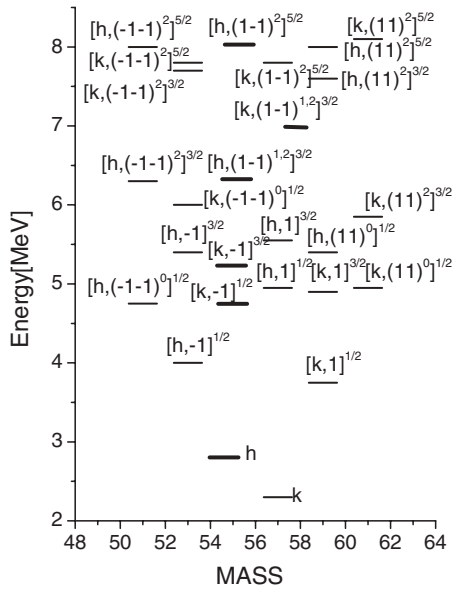

FIG. 6. Odd-mass states around $A = 58$. The depicted states are constructed by coupling one- and two-phonon states to $k = 3p_{3/2}$ and $h = 3f_{7/2}$ single-particle states. The total isospin of the states is given in the upper right-hand corner of the square bracket of each configuration.

above for $A = 52, 56, 60$. The $T = \frac{5}{2}$ states display a fairly constant energy, close to the theoretical value $e_j + \omega_1^{01\alpha} + \omega_1^{01\beta}$. This is also the case for $T = \frac{3}{2}$ states obtained by coupling a particle creation operator to two removal phonons or a hole annihilation operator to two addition bosons. However, the energies of the $T = \frac{1}{2}$ states in which the annihilation operator $a_{\frac{7}{2}^-}$ is coupled with the two removal bosons, or the creation operator $a^+_{\frac{3}{2}^-}$ with the two addition phonons, are systematically lowered presumably because of the same reason as for the $T = 0$ states in $A = 52, 60$ nuclei and for the $T = \frac{1}{2}$ particle-vibration states in Table VII for $A = 53, 59$ nuclei. The evidence is again completely symmetrical with respect to $A = 56$. The alternate between the ground state spins $\frac{7}{2}$ and $\frac{3}{2}$ in odd nuclei is also consistent with the coupling scheme.

The model allows us to identify a number of states belonging to the same IAS sequences with $T = \frac{1}{2}, 1, \frac{3}{2}, 2, \frac{5}{2}$. Their excitation energy is reproduced within 40 keV. This is a test for the coefficient of the Coulomb term in Eq. (2).

Figure 7 shows the experimental information on two-phonon states with $I^\pi = 1^+$. The data support the vibrational picture described previously. The energies of the states that we identified as two phonons in $A = 52, 56, 60$ are indeed similar to the ones given by the sum of IVP and ISP phonons in $A = 54$ and $A = 58$.

APPENDIX B: EQUATIONS DETERMINING RPA ENERGIES AND AMPLITUDES

In this Appendix we summarize the conventional RPA equations that are used in the calculation. Assuming the interactions in Eq. (6), the frequencies and amplitudes are

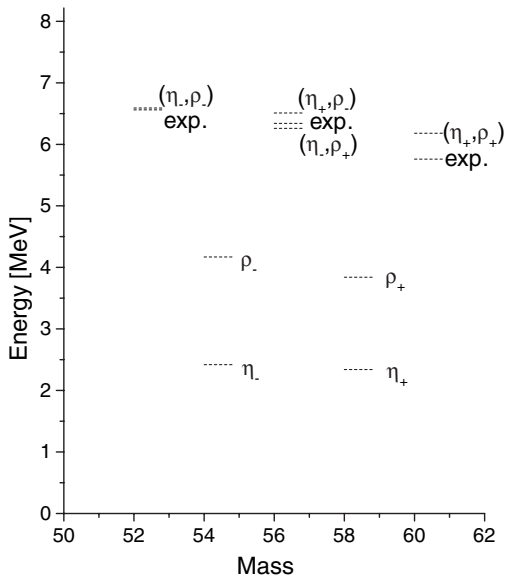

FIG. 7. $I^\pi = 1^+$ states around $A = 56$. The set of quantum numbers of each phonon is given by the short notation, $\eta = \Gamma^+(IM, TT_z, \alpha, \nu)$, $\rho = \Gamma^+(IM, TT_z, \alpha, \nu)$.

obtained from the equations

$$\frac{1}{g^{IT\alpha}} = \left(\frac{\left(f^{IT\alpha}_{j_1 j_2}\right)^2}{e_{j_1} + e_{j_2} - \omega^{IT\alpha}_\nu} + \frac{\left(f^{IT\alpha}_{j_1 j_2}\right)^2}{e_{j_1} + e_{j_2} + \omega^{IT\alpha}_\nu} \right), \tag{B1}$$

$$\lambda^{IT\alpha}_{\nu;j_1 j_2} = \frac{\Xi^{IT\alpha}_\nu \, f^{IT\alpha}_{j_1 j_2}}{e_{j_1} + e_{j_2} - \omega^{IT\alpha}_\nu}; \quad \mu^{IT\alpha}_{\nu;j_1 j_2} = \frac{\Xi^{IT\alpha}_\nu \, f^{IT\alpha}_{j_1 j_2}}{e_{j_1} + e_{j_2} + \omega^{IT\alpha}_\nu}, \tag{B2}$$

while the vertex factors are given by

$$\Xi^{IT\alpha}_\nu = \left(\frac{\left(f^{IT\alpha}_{j_1 j_2}\right)^2}{\left(e_{j_1} + e_{j_2} - \omega^{IT\alpha}_\nu\right)^2} - \frac{\left(f^{IT\alpha}_{j_1 j_2}\right)^2}{\left(e_{j_1} + e_{j_2} + \omega^{IT\alpha}_\nu\right)^2} \right)^{-1/2}. \tag{B3}$$

APPENDIX C: RENORMALIZATION OF THE GT TRANSITIONS

Renormalization diagrams (Fig. 3) are of the same order as the original ones. In this Appendix we show how to calculate them. The procedure is not restricted to cases in which the energies of the initial and final states are much smaller than the frequency of the giant resonance, for which the notion of a fixed effective charge may be applicable.

1. Bare matrix elements

Let us consider a diagram in which the successive states are labeled by the integer $i (i = 0, 1, 2, \ldots, m, n, \ldots, u)$. Thus $|0\rangle$ and $|u\rangle$ represent initial and final states, respectively. A neutron particle line is transformed into a proton one through the GT operator Q_{1M} between the $|m\rangle = |[c^+_k X_k]^0\rangle$ and the $|n\rangle = |[b^+_{k'} X_k]^1_M\rangle$ states (Fig. 3, diagram 1). The results will be independent of the nature of the intermediate state $|X_k\rangle$. All states labeled by $0 \leqslant i \leqslant m$ carry $I = 0$, $T = 1$, $M_T = -1$; while those with $n \leqslant i \leqslant u$ carry $I = 1$, $0 \leqslant T \leqslant 2$ $M_T = 0$. For each time permutation, the bare matrix element reads

$$\begin{aligned} \langle u|Q_{1M}|0\rangle_{\text{bare}} &= W \left\langle [b^+_{k'} X_k]^1_q \middle| Q_{1M} \middle| [c^+_k X_k]^0 \right\rangle D_u \, D_0 \\ &= -W \, \frac{\langle k'||\sigma||k\rangle}{\sqrt{6}\hat{k}} \, D_u \, D_0, \end{aligned} \tag{C1}$$

where

$$\begin{aligned} W &= \langle u|V|u-1\rangle \cdots \langle n+1|V|n\rangle \langle m|V|m-1\rangle \cdots \langle 1|V|0\rangle, \\ D_0 &= \Pi_{i=1}^{i=m} \frac{1}{e_0 - e_i}, \qquad D_u = \Pi_{i=n}^{i=u-1} \frac{1}{e_u - e_i}. \end{aligned} \tag{C2}$$

2. Renormalized matrix elements

The collective form of the GT operator is given in Eq. (8). In the first place we calculate the contributions through which the phonon is created before the state $|m\rangle$ and annihilated through a particle-vibration vertex at the point at which the bare GT

vertex was previously inserted (see Fig. 3, diagram 2)

$$\langle u|\,(Q_{1M})_{\rm coll}\,|0\rangle = W\,\langle n|H_{\rm pv}|m\,\Gamma^{+}_{1M,11,0;1}\rangle \times \langle\Gamma^{+}_{1M,11,0;1}|\,(Q_{1M})_{\rm coll}\,|\,\rangle\,D_u\,\Sigma^{(0)} = -W\,\frac{\left(\Xi^{110}_1\right)^2}{g^{110}}\,\frac{\langle k'||\sigma||k\rangle}{2\,\hat{k}}\,D_u\,\Sigma^{(0)}, \quad \text{(C3)}$$

where

$$\Sigma^{(0)} \equiv \frac{1}{\left(e_u - e_m - \omega^{110}_1\right)(e_0 - e_m)(e_0 - e_{m-1})\cdots(e_0 - e_1)} + \frac{1}{\left(e_u - e_m - \omega^{110}_1\right)\left(e_u - e_{m-1} - \omega^{110}_1\right)(e_0 - e_{m-1})\cdots(e_0 - e_1)} + \cdots + \frac{1}{\left(e_u - e_m - \omega^{110}_1\right)\left(e_u - e_{m-1} - \omega^{110}_1\right)\cdots\left(e_u - e_0 - \omega^{110}_1\right)} = D_0\,\frac{1}{e_u - e_0 - \omega^{110}_1}. \quad \text{(C4)}$$

Similarly, we calculate the contributions due to the creation of the $\Gamma^{+}_{1(-M),1(-1),0;1}$ phonon between the m and n states, and its annihilation at later times (Fig. 3, diagram 3). Proceeding as in Eq. (C4), we obtain

$$\langle u|\,(Q_{1M})_{\rm coll}\,|0\rangle = W\,\langle n|H_{\rm pv}|m\,\Gamma^{+}_{1M,11,0;1}\rangle \times \langle\,|\,(Q_{1M})\,|\Gamma^{+}_{1(-M),1(-1),0;1}\rangle\,D_0\,\Sigma^{(u)} = -W\,\frac{(\Xi^{110})^2}{g^{110}}\,\frac{\langle k'||\sigma||k\rangle}{2\hat{k}}\,D_0\,\Sigma^{(u)},$$

$$\Sigma^{(u)} = D_u\,\frac{1}{e_0 - e_u - \omega^{110}_1}. \quad \text{(C5)}$$

Addition of Eqs. (C3) and (C5) yields the total renormalized value of the GT matrix element

$$\langle u|Q_{1M}|0\rangle_{\rm ren} = \langle u|Q_{1M}|0\rangle_{\rm bare} \times \left(1 - \frac{\left(\Xi^{110}_1\right)^2}{g^{110}}\,\frac{2\omega^{110}_1}{(e_u - e_0)^2 - \left(\omega^{110}_1\right)^2}\right), \quad \text{(C6)}$$

where the bare matrix element is given in Eq. (C1). In the limit $\omega^{110} \gg |e_u - e_0|$, the usual constant effective charge is reproduced. In Eq. (C6) the effective charge depends on the relative value of the phonon energy and the transition energy, since the factor multiplying the bare matrix element is less than unity for low-lying transitions but greater than unity for transitions populating states higher than the giant resonance. If $|e_u - e_0| \approx \omega^{110}_1$, perturbation theory is not applicable.

3. Special case: Population of the GTR

Here we deal with the final state

$$|u\rangle = [\Gamma^{+}_{1M,1,0;1}\Gamma^{+}_{00,1,1;1}]^T\,|\rangle, \quad \text{(C7)}$$

with one GT phonon more than the initial state. In such a case, Eq. (C6) is not valid since, according to Fig. 3, diagram 4, the first intermediate state is the same as the final state. In this case, the rules for calculating perturbatively the amplitudes of initial and final states are different from those used in Eq. (C6). Therefore we must (i) eliminate from Eq. (C4) the contribution corresponding to this particular time ordering and (ii) replace it by a calculation using the appropriate amplitude of the final state $|u\rangle$.

The first step is accomplished through the substitution

$$\Sigma^{(0)} \to \Sigma^{(0)'} = \Sigma^{(0)} - \Pi_{0\leqslant i\leqslant m}\,\frac{1}{e_u - e_i - \omega^{110}_1} = \frac{D_0 - C_0}{e_u - e_0 - \omega^{110}_1} = D_0\,S_0, \quad \text{(C8)}$$

where

$$C_0 \equiv \Pi^{i=m}_{i=1}\,\frac{1}{e_u - e_i - \omega^{110}_1} = D_0 + \left(e_u - e_0 - \omega^{110}_1\right)\left.\frac{d\,C_0}{d\,e_u}\right|_{e_u = e_0 + \omega^{110}_1} + \cdots = D_0\left[1 - \left(e_u - e_0 - \omega^{110}_1\right)\,S_0 + \cdots\right],$$

$$S_0 \equiv \sum_{i=1}^{i=m}\frac{1}{e_0 - e_i}, \quad \text{(C9)}$$

while Eq. (C5) reads

$$\Sigma^{(u)} = -\frac{1}{2\omega^{110}_1}\,D_u\,. \quad \text{(C10)}$$

Therefore, Eq. (C6) should be substituted by

$$\langle u|Q_{1M}|0\rangle^{(1)}_{\rm ren} = \langle u|Q_{1M}|0\rangle'_{\rm bare} \times \left[1 + \frac{\left(\Xi^{110}_1\right)^2}{g^{110}}\left(S_0 - \frac{1}{2\omega^{110}_1}\right)\right]. \quad \text{(C11)}$$

Note that unlike the case of Eq. (C6), the renormalization factor in Eq. (C11) changes with the time permutations of the bare diagram, since S_0 depends on it. This is indicated by primes in Eq. (C11). Note also that the population of a final state $|u\rangle$

with a definite isospin value requires the linear combination in Eq. (15).

To accomplish the second step, we must add to Eq. (C11) the contribution due to the creation of the GT phonon during the initial state $|0\rangle$ (Fig. 3, diagram 4). The amplitude of the final unperturbed state is modified as [16]

$$|u\rangle_{\rm ren} = |u\rangle_{\rm bare}\left(1+\frac{1}{2}\frac{d\Delta}{de_u}\right), \tag{C12}$$

where Δ is the contribution to the energy of the final state, obtained from the section of Fig. 3 diagram 4 between the two identical states. The energies Δ are obtained as follows:

We first perform the calculation between projected states

$$|u_{t_z}\rangle \equiv \Gamma^+_{1M,1t_z,0;1}\Gamma^+_{00,1(-t_z),1;1}]\,|\rangle\,. \tag{C13}$$

We obtain the energy matrix elements $\Delta_i(t_z,t'_z)$, where t_z (t'_z) is the isospin projection of the initial (final) GT phonon. The corresponding energy diagrams are represented in Fig. 5 for the three cases of interest F, G, H. Since the states $|u_{t_z}\rangle$ have total isospin projection $T_z=0$, the isospin projection of the pairing phonon is also determined.

We note the following symmetries

$$\Delta_i(t_z,t'_z) = \Delta_i(-t_z,-t'_z) = \Delta_i(t'_z,t_z), \tag{C14}$$

and we define

$$\begin{aligned}
\Delta_F &\equiv \Delta_F(1,1) = 2\Delta_F(0,0) = -2\Delta_F(1,0),\\
\Delta_G &= 2\Delta_G(0,0) = \Delta_G(1,0),\\
\Delta_H &= \Delta_H(1,-1) = 2\Delta_H(0,0) = -2\Delta_H(1,0).
\end{aligned} \tag{C15}$$

All other $\Delta_i(t_z,t'_z)$ vanish.

The energy matrix element between states with good T reads

$$\begin{aligned}
\Delta^T_{T_z=0} &= 2\langle 11;1(-1);T0\rangle^2\Delta_i(1,1)\\
&\quad +4\langle 11;1(-1);T0\rangle\langle 10;10;T0\rangle\Delta_i(1,0)\\
&\quad +\langle 10;10;T0\rangle^2\Delta_i(0,0)+2\,(-1)^T\\
&\quad \times\langle 11;1(-1);T0\rangle^2\Delta_i(1,-1)\\
&= (1-r_T)\left(\Delta_F+(-1)^T\Delta_H\right)+r_T\,\Delta_G,
\end{aligned} \tag{C16}$$

where we have used Eqs. (C14) and (C15) and r_T is defined in Eq. (16). We have thus shown that the renormalization contribution to the amplitude of the state $|u\rangle$ undergoes the same isospin transformation as the bare matrix element in order to populate two phonon states with definite isospin.

Let us calculate now the expression for $\frac{1}{2}\frac{d\Delta^T}{de_u}$. The diagrammatic calculation of $\Delta_i(t_z,t'_z)$ yields

$$\begin{aligned}
\Delta_i(t_z,t'_z) &= W\langle n|H_{\rm pv}|m\,\Gamma^+(1q,11,0)\rangle D_u\,C_0\\
&= W\frac{\langle k'||\sigma||k\rangle}{\sqrt{6}\hat{k}}\,\Xi^{110}_1\,D_u\,C_0.
\end{aligned} \tag{C17}$$

Therefore

$$\begin{aligned}
\frac{1}{2}\frac{d\,\Delta_i(t_z,t'_z)}{d\,e_u} &= \frac{1}{2}W\,\Xi^{110}_1\frac{\langle k'||\sigma||k\rangle}{\sqrt{6}\hat{k}}\left(\frac{d\,D_u}{d\,e_u}\,C_0+D_u\,\frac{d\,C_0}{d\,e_u}\right)\\
&= -\frac{1}{2}W\,\Xi^{110}_1\frac{\langle k'||\sigma||k\rangle}{\sqrt{6}\hat{k}}\,D_u\,D_0\,(S_u+S_0)\\
&= -\frac{1}{2}\Xi^{110}_1\langle u|Q_{1,M}|0\rangle'_{\rm bare}\,(S_u+S_0)\,,
\end{aligned} \tag{C18}$$

where Eq. (C1) is used with primes [defined as in Eq. (C11)], S_0 is defined in Eq. (C9), and

$$S_u \equiv \sum_{i=n}^{i=u-1}\frac{1}{e_u-e_i}. \tag{C19}$$

We are now in the position to calculate the renormalized values of κ_i [Eq. (14)]. Using Eqs. (C11) and (C18)

$$\begin{aligned}
(\kappa_i)_{\rm ren} &= \langle u|Q_{1M}|0\rangle^{(1)}_{\rm ren}\;+\;\langle\Gamma^+_{1M,11,0;1}|Q_{1M}|\rangle\,\frac{1}{2}\frac{d\Delta_i}{de_u}\\
&= \langle u|Q_{1M}|0\rangle'_{\rm bare}\left[1+\frac{(\Xi^{110})^2}{2g^{110}}\left(S_u-S_0+\frac{1}{\omega^{110}}\right)\right].
\end{aligned} \tag{C20}$$

The value of these expressions is given in Table VI (rows F, G, and H). Therefore, expression (20) for the intensity of the transition to the resonant state with a definite value of T and expression (21) for the sum of these intensities over all values of T are still valid, provided we replace the bare amplitudes κ_{i1} by the renormalized ones Eq. (C20).

APPENDIX D: IKEDA SUM RULE REVISITED

In this Appendix we study the extent to which Eq. (22) is satisfied in schematic models treated within the NFT framework. Let us consider first the simple case of a single l shell and assume that there are two neutrons coupled to zero angular momentum in the (lowest) single-particle state with $h=k+1=l+\frac{1}{2}(|0\rangle=[c^+_hc^+_h]^0|\rangle)$. There are no states excited by the operator $\bar{Q}_{1,M}$, while the population of the states $|a\rangle=|[c^+_hb^+_h]^1_M\rangle$ and $|b_\pm\rangle=\frac{1}{\sqrt{2}}(|[c^+_kb^+_h]^1_M\rangle\pm|[b^+_kc^+_h]^1_M\rangle)$ through the operator Q_{1M} satisfies the sum rule

$$\begin{aligned}
&|\langle a|Q_{1M}|0\rangle|^2\;+|\langle b_+|Q_{1M}|0\rangle|^2\;+\;|\langle b_-|Q_{1M}|0\rangle|^2\\
&\quad =1.13+0.44+0.44=2.
\end{aligned} \tag{D1}$$

At least as relevant to the study of ^{58}Ni is to assume that states h are filled and that there are two coupled k neutrons in the ground state ($|0\rangle=|[c^+_kc^+_k]^0|\rangle$). Since a Gamow-Teller interaction is included, we may apply expressions given in Appendix B for the GT phonons. We obtain

$$g=\frac{3(\epsilon^2-\omega^2)}{8}\hat{k}^2\epsilon,\quad \Xi=\frac{\sqrt{3}(\omega^2-\epsilon^2)}{4\hat{k}\sqrt{\epsilon\omega}},\quad \frac{\Xi^2}{g}=\frac{\epsilon^2-\omega^2}{2\omega}, \tag{D2}$$

where we have dropped the indices I, T, α, and ν from g, Ξ, and ω. Moreover, since ours will be a first-order calculation in

TABLE VIII. Values of the amplitudes used in Eqs. (D6) and (D8). Here $\alpha_{\rm ren} = \alpha_{\rm bare} \times$ fac.

	α_k	α_h	β_k	β_h
Bare	$-g/3\omega$	$-4g/3(\epsilon+\omega)$	$g/3\omega$	$4g/3(\omega-\epsilon)$
Fac	$1+\epsilon^2/\omega^2$	$1+(\epsilon-\omega)(2\omega+\epsilon)/4\omega^2$	$1+\epsilon^2/\omega^2$	$1-(\epsilon+\omega)(2\omega-\epsilon)/4\omega^2$

the NFT expansion parameter $1/k$, we use the leading values $\langle k||\sigma||k\rangle^2 = 2\hat{k}^2$ and $\langle k||\sigma||h\rangle^2 = 4\hat{k}^2(\hat{k} = \sqrt{k+1/2})$.

The first diagrammatic contribution $\mathcal{O}(k^0)$ is represented in Fig. 2, diagram A. The bare and renormalized matrix elements are

$$\langle [c_k^+ b_k^+]^1_M | Q_{1M} | 0\rangle_{\rm bare} = \langle k||\sigma||k\rangle/\hat{k}\sqrt{3},$$
$$\left\langle [c_k^+ b_k^+]^1_M | Q_{1M} | 0\right\rangle_{\rm ren} = \left\langle [c_k^+ b_k^+]^1_M | Q_{1M} | 0\right\rangle_{\rm bare} \left(1 + \frac{2\Xi^2}{g\omega}\right), \tag{D3}$$

$$|\langle [c_k^+ b_k^+]^1_M | Q_{1M} | 0\rangle|^2 = \frac{2}{3} \text{ (bare) or}$$
$$= \frac{2\epsilon^4}{3\omega^4} \text{(renormalized).} \tag{D4}$$

Use has been made of Eq. (C6) with $\epsilon_u = \epsilon_0$ for the calculation of the renormalization factor.

There are no more diagrams of $\mathcal{O}(k^0)$ corresponding to the GT transition. However, as indicated in Eq. (20), the collective operator may act as an amplifier for diagrams of $\mathcal{O}(k^{-1})$ populating the GTR.

$$\langle \Gamma^+_{1M}[c_k^+ c_k^+]^0 | Q_{1M} | 0\rangle_F$$
$$= \frac{\Xi}{g}\left(1 + \frac{1}{2}\frac{\partial \Delta_F}{\partial e_u}\right) + \langle \Gamma^+_{1M}[c_k^+ c_k^+]^0 | Q_1 | 0\rangle_F$$
$$= \frac{\Xi}{g}(1 + \alpha_k + \alpha_h), \tag{D5}$$

$$|\langle \Gamma^+_{1M}[c_k^+ c_k^+]^0 | Q_{1M} | 0\rangle_F|^2 - \frac{\Xi^2}{g^2}$$
$$= \frac{2\Xi^2}{g^2}(\alpha_k + \alpha_h) = \frac{1}{3}\left(5 - 4\frac{\epsilon}{\omega} - \frac{\epsilon^2}{\omega^2}\right) \text{ (bare) or}$$
$$= 1 - \frac{1}{3}\left(\frac{\epsilon}{\omega} + \frac{\epsilon^3}{\omega^3} + \frac{\epsilon^4}{\omega^4}\right) \text{ (renormalized),} \tag{D6}$$

where the subindex F indicates those diagrams included in Fig. 5. The subindex k indicates time-ordering for which all fermion lines represent particles; the subindex h those for which there is a hole line. They yield the values listed in Table VIII. Similar calculations hold for the operator $\bar{Q}_{1M}$.

$$\langle \bar{\Gamma}^+_{1M}[c_k^+ c_k^+]^0 | \bar{Q}_{1M} | 0\rangle_G = \frac{\Xi}{g}(1 + \beta_k + \beta_h), \tag{D7}$$

$$-|\langle \bar{\Gamma}^+_{1M}[c_k^+ c_k^+]^0 | \bar{Q}_{1M} | 0\rangle_G|^2 + \frac{\Xi^2}{g^2}$$
$$= -\frac{2\Xi^2}{g^2}(\beta_k + \beta_h) = \frac{1}{3}\left(5 + 4\frac{\epsilon}{\omega} - \frac{\epsilon^2}{\omega^2}\right) \text{ (bare) or}$$
$$= 1 + \frac{1}{3}\left(\frac{\epsilon}{\omega} + \frac{\epsilon^3}{\omega^3} - \frac{\epsilon^4}{\omega^4}\right) \text{ (renormalized).} \tag{D8}$$

Therefore the contribution of Eq. (D6) plus Eq. (D8) to the sum rule (22) is

$$\frac{2}{3}\left(5 - \frac{\epsilon^2}{\omega^2}\right) \text{ (bare)} \quad \text{or} \quad 2\left(1 - \frac{\epsilon^4}{3\omega^4}\right) \text{ (renormalized).} \tag{D9}$$

Addition of Eqs. (D4) and (D9) yields the values

$$\frac{2}{3} + \frac{2}{3}\left(5 - \frac{\epsilon^2}{\omega^2}\right) = 4 - \frac{2\epsilon^2}{3\omega^2} \text{ (bare),}$$
$$\frac{2\epsilon^4}{3\omega^4} + 2\left(1 - \frac{\epsilon^4}{3\omega^4}\right) = 2 \text{ (renormalized).} \tag{D10}$$

The above contributions are displayed in Fig. 8 as functions of ϵ/ω. The calculation takes care of the blocking effects in the creation of the GT phonon in the presence of the two k particles through the term β_h, which becomes dominant at least in the limit $\omega \to \epsilon$. We also notice the importance

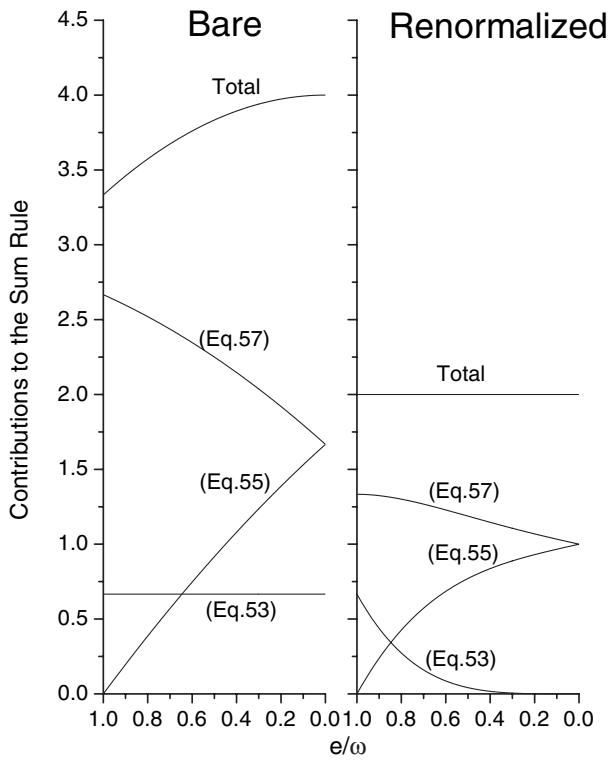

FIG. 8. Bare and renormalized contributions to the Ikeda sum rule. The contributions are displayed as functions of the variable ϵ/ω. The corresponding expressions are quoted on each curve. The sum of contributions is the curve labeled *total*. The values of $\alpha_{k(h)}$ and $\beta_{k(h)}$, which appear in these equations, are taken from Table VIII.

of the renormalization diagrams. The curves of Fig. 8 are self-explanatory of the relevance of the renormalization and of the subtle competition between the processes included in the diagrammatic treatment.

[1] H. Ejiri, Phys. Rep. **338**, 265 (2000).
[2] D. J. Horen *et al*., Phys. Lett. **B99**, 383 (1981).
[3] K. Hara *et al*., Phys. Rev. C **68**, 064612 (2003).
[4] H. Fujita *et al*., Phys. Rev. C **75**, 034310 (2007).
[5] S. El-Kateb *et al*., Phys. Rev. C **49**, 3128 (1994).
[6] Y. Fujita *et al*., Phys. Rev. C **70**, 054311 (2004).
[7] A. Bohr and B. R. Mottelson, *Nuclear Structure*, Vol. II. (W. A. Benjamin, Massachussetts, 1975), Chap. 6.
[8] A. Arima, Nucl. Phys. **A649**, 260 (1999).
[9] A. Arima, K. Shimizu, W. Bentz, and H. Hyuga, Adv. Nucl. Phys. **18**, 1 (1987).
[10] E. Caurier, K. Langanke, G. Martinez-Pinedo, and F. Nowacki, Nucl. Phys. **A653**, 439 (1999).
[11] E. Caurier, G. Martinez-Pinedo, F. Nowacki, A. Poves, J. Retamosa, and A. P. Zuker, Phys. Rev. C **59**, 2033 (1999); see also Sec. VI of Ref. [4].
[12] D. R. Bes, R. A. Broglia, O. Hansen, and O. Nathan, Phys. Rep. **34C**, 1 (1977).
[13] D. R. Bes, G. G. Dussel, R. A. Broglia, R. J. Liotta, and B. R. Mottelson, Phys. Lett. **B52**, 253 (1974).
[14] D. R. Bes, R. A. Broglia, G. G. Dussel, and R. J. Liotta, Phys. Lett. **B56**, 109 (1975).
[15] G. G. Dussel, E. C. Seva, and H. M. Sofia, Phys. Rev. C **49**, 1989 (1994).
[16] D. R. Bes, G. G. Dussel, and H. M. Sofia, Am. J. Phys. **45**, 191 (1977).